Yuzuncu Yil University
Journal of the Institute of Natural & Applied Sciences

https://dergipark.org.tr/en/pub/yyufbed

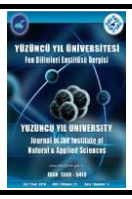

Research Article

Gamma Radiation Shielding Efficiency of High Entropy Alloys: A Comparative Study

Ufuk PERİŞANOĞLU*

Hakkari University, Engineering Faculty, Materials Science and Engineering Department, 30000, Hakkari, Türkiye
Ufuk PERİŞANOĞLU, ORCID No: 0000-0003-4110-2241
*Corresponding author e-mail: ufukperisanoglu@hakkari.edu.tr

Article Info

Received: 07.06.2024
Accepted: 10.07.2024
Online August 2024

DOI:10.53433/yyufbed.1497606

Keywords
Buildup factor,
Effective atomic number,
Gamma shielding,
Half-value layer,
High entropy alloys,
Mass attenuation coefficient

Abstract: High entropy alloys (HEAs) represent a novel class of materials characterized by their unique composition of four or more principal elements in near-equiatomic ratios, offering exceptional properties for various applications. This study investigates the gamma radiation shielding parameters of selected HEAs, namely FeCoNiCrMn, TaNbHfZrTi, NbMoTaW, AlMoNbV, and NbTaTiV. Mass attenuation coefficients (MAC) were calculated by using EpiXS program over a photon energy range of 0.015-15 MeV and these results were verified using with the WinXCOM software. The results show that the MAC values are highest at low photon energies due to the photoelectric effect, with notable peaks corresponding to the K-shell absorption edges of specific elements. At photon energy of 0.015 MeV, the MAC values for the FeCoNiCrMn, TaNbHfZrTi, NbMoTaW, AlMoNbV, and NbTaTiV alloys are 57.6, 90.4, 98.9, 27.8, and 81.5 cm²/g, respectively. Among these alloys, NbMoTaW exhibits the highest MAC value, whereas AlMoNbV displays the lowest. The half-value layer (HVL) and mean free path (MFP) values were also found thinner for NbMoTaW at all of the photon energies. Additionally, the effective atomic number (Z_{eff}) and exposure buildup factors (EBF) were analyzed. The results demonstrate that NbMoTaW and TaNbHfZrTi, offer superior radiation shielding capabilities compared to conventional shielding materials, with higher usability in environments subjected to gamma radiation. These findings underscore the promise of HEAs in advanced shielding applications, showcasing their ability to enhance safety and performance in sectors with high demands.

Yüksek Entropili Alaşımların Gama Radyasyonundan Koruma Etkinliği: Karşılaştırmalı Bir Çalışma

Makale Bilgileri

Geliş: 07.06.2024
Kabul: 10.07.2024
Online Ağustos 2024

DOI:10.53433/yyufbed.1497606

Anahtar Kelimeler
Birikim faktörü,
Etkin atom numarası,
Gama zırhlama,
Kütle azaltma katsayısı,
Yarı değer kalınlığı,
Yüksek entropili alaşımlar

Öz: Yüksek entropili alaşımlar (HEA'lar), yaklaşık eşit oranlarda dört veya daha fazla temel elementin benzersiz bileşimiyle karakterize edilen ve çeşitli uygulamalar için olağanüstü özellikler sunan yeni bir malzeme sınıfını temsil eder. Bu çalışma, FeCoNiCrMn, TaNbHfZrTi, NbMoTaW, AlMoNbV ve NbTaTiV gibi seçili HEA'ların gama zırhlama parametrelerini araştırmaktadır. EpiXS programı kullanılarak 0.015-15 MeV enerji aralığında kütle azaltma katsayıları (MAC) hesaplanmış ve bu sonuçlar WinXCOM yazılımı ile doğrulanmıştır. Bulgular, MAC değerlerinin, fotoelektrik etki nedeniyle düşük foton enerjilerinde en yüksek olduğunu ve belirli elementlerin K-soğurma kıyılarına karşılık gelen belirgin pikler gösterdiğini ortaya koymaktadır. 0,015 MeV foton enerjisinde, FeCoNiCrMn, TaNbHfZrTi, NbMoTaW, AlMoNbV ve NbTaTiV alaşımları için MAC değerleri sırasıyla 57.6, 90.4, 98.9, 27.8 ve 81.5 cm²/g'dır. Bu alaşımlar arasında NbMoTaW en yüksek MAC değerini sergilerken, AlMoNbV en düşük değeri göstermektedir. Yarı kalınlık (HVL) ve ortalama serbest yol (MFP) değerleri de tüm foton enerjilerinde NbMoTaW için daha ince bulunmuştur. Ayrıca, etkin atom numarası (Z_{eff}) ve maruz kalma

birikim faktörleri (EBF) de analiz edilmiştir. Sonuçlar, NbMoTaW ve TaNbHfZrTi'nin, geleneksel koruma malzemelerine kıyasla üstün radyasyon koruma yetenekleri sunduğunu ve gama radyasyonuna maruz kalan ortamlarda daha yüksek kullanılabilirlik sağladığını göstermektedir. Bu bulgular, HEA'ların gelişmiş zırhlama uygulamalarında vaat ettiklerinin altını çizerek, yüksek taleplerin olduğu sektörlerde güvenlik ve performansı artırma yeteneklerini ortaya koymaktadır.

1. Introduction

High entropy alloys (HEAs) mark a notable departure from traditional alloy design. These alloys are different because they consist of five or more elements mixed in nearly equal proportions, rather than having a single primary metal with small amounts of other elements added. This design strategy leads to a high mixing entropy. As a result, HEAs exhibit a unique combination of properties, such as increased strength, hardness, and improved resistance to wear and corrosion (Buluc et al., 2017; Filho et al., 2020; Yaykaşlı, et al., 2023a). These alloys are especially valuable for their potential use in environments that face extreme conditions, such as high temperatures and corrosive settings. The distinctive makeup of HEAs contributes to markedly improved properties, including impact resistance, stability at high temperatures, and biocompatibility (Socorro-Perdomo et al., 2021).The wide range of possible alloy combinations also results in an unparalleled variety of configurations, allowing properties to be customized to meet specific engineering requirements. The field has experienced rapid growth, driven by international collaborations and scientific workshops to share recent advances and explore future research avenues. For example, a major international workshop held in China in 2014 aimed to enhance discussions on scientific challenges and identify critical areas for further development of HEAs (Lu et al., 2015).

As knowledge of HEAs deepens, attention has shifted from simply grasping their fundamental properties to investigating their practical uses. These include applications in ballistic protection and potential uses in the aerospace and automotive industries, which capitalize on their superior mechanical properties and resistance to deformation under stress (Filho et al., 2020).

High entropy alloys thus emerge as a promising category of materials that defy conventional metallurgical methods with their innovative properties and extensive potential for application across various high-demand sectors. Continuing the exploration of high entropy alloys (HEAs), these materials are distinguished by their inherent ability to endure harsh operating conditions. A key characteristic of HEAs is their outstanding high-temperature properties, making them ideal for use in turbine blades in jet engines and components in nuclear reactors. These alloys maintain a stable microstructure at high temperatures, preserving their strength and resisting oxidation and wear for long durations (Müller et al., 2019; Ren et al., 2022).

Research has further demonstrated the adaptability of HEAs by incorporating elements such as Yttrium, which significantly boosts mechanical properties by refining the microstructure and improving phase stability. This type of elemental adjustment creates opportunities to tailor alloys for specific performance requirements, offering customized solutions for industries needing materials with highly specialized performance characteristics (Ren et al., 2022). The field of HEAs is also branching into the area of amorphous alloys, applying the high entropy concept to non-crystalline materials. These high entropy amorphous alloys (HEAAs) are attracting interest for their ability to merge the advantages of amorphous materials (i.e high strength and soft magnetic properties) with the thermal stability and resistance to crystallization typical of the high entropy approach (Tunes et al., 2023).Overall, high entropy alloys embody a dynamic area within materials science that consistently extends the limits of alloy design and applications. Their evolution is driven by both theoretical understanding and experimental breakthroughs, opening up promising new pathways for advancements in materials technology.

Recently, many studies have been conducted on the usability of HEAs in nuclear applications. Lu et al. successfully synthesized Ti2ZrHfV0.5Mo0.2 and investigated its suitability for nuclear applications in detail. The results obtained indicate that the displacement damage (dpa: Displacement

per atom) of the synthesized HEA has a small value of 0.03 and is promising as an alternative to currently used nuclear materials (Lu et al., 2019). Jia et al. successfully synthesized TiVNbTa HEA and investigated its suitability for nuclear applications under He bombardment. Their results showed that TiVNbTa refractory alloy has a small enough dpa (0.3) value to be promising for nuclear applications (Jia et al., 2021).

In another study, Zhang et al. (2021) calculated the radiation resistance of Mo0.5NbTiVCr0.25 and Mo0.5NbTiV0.5Zr0.25 refractory alloys with He ion radiation. Both refractory alloys were found to have high radiation resistance and are promising for nuclear applications. Ferreirós et al. (2023) synthesized VNbCrMo refractory alloy using arc melting method and neutron absorption properties were investigated. The results showed that VNbCrMo refractory alloy has the potential to be used for nuclear applications. In other study on boron nitride nanosheet-reinforced WNiCoFeCr HEAs demonstrated significant improvements in structural, physical, mechanical, and radiological shielding properties with the addition of B4C, making them suitable for radiation protection applications (Kavaz et al., 2022). Yaykaşlı et al. (2023b) produced a new high-entropy alloy, CoCrFeNiAg, and determined its radiation shielding properties experimentally using a ^{137}Cs source and a NaI(Tl) detector system. The results showed that HEA has excellent radiation shielding properties and these properties are promising for use in nuclear technology and the radiation industry. They also showed that the crystal size decreases with increasing alloying time and the synthesized alloy exhibits thermal stability over a wide temperature range.

In this study, the gamma radiation shielding parameters of some HEAs, i.e "FeCoNiCrMn, TaNbHfZrTi, NbMoTaW, AlMoNbV and NbTaTiV (Shang et al., 2021)" were comprehensively evaluated, MAC, HVL, MFP, Z_{eff} and buildup factors of selected HEAs in the photon energy range of 0.015-15 MeV were obtained and the results were evaluated in terms of radiation shielding.

2. Material and Methods

The mass attenuation coefficient (MAC) quantifies the likelihood of interaction per unit mass for a given shielding material. It is formulated according to the Beer-Lambert law, as shown in Equations 1 and 2 (Rammah et al., 2020).

$$MAC = \mu_m = \frac{\mu}{\rho} = \frac{1}{\rho t}\ln\left(\frac{I}{I_0}\right) \tag{1}$$

$$I = I_0\, e^{-\mu t} \tag{2}$$

In these equations I_0 represents the incident photon intensity, I denotes the attenuated photon intensity, and t is the thickness of the sample. The linear attenuation coefficient is denoted by μ, while μ/ρ represents the mass attenuation coefficient.

Another shielding parameter related to the linear attenuation coefficient is the mean free path (MFP), which is the average distance a photon travels through a material before interacting. The MFP is determined by Equation 3 (Yıldız Yorgun, 2019).

$$MFP = 1/\mu \tag{3}$$

The half-value layer (HVL) is the thickness of material required to attenuate radiation intensity by half. The HVL can be calculated using Equation 4 (Issa et al., 2020).

$$HVL = \frac{ln2}{\mu} \tag{4}$$

Composite materials, which consist of multiple elements, contain a large number of atoms and electrons at a specific energy level. In such cases, the effective atomic number (Z_{eff}) can be calculated using Equation 5 (Perişanoğlu et al., 2020).

$$Z_{eff} = \frac{\sum_i f_i A_i \left(\frac{\mu}{\rho}\right)_i}{\sum_j \frac{A_j}{Z_j} \left(\frac{\mu}{\rho}\right)_j} \quad (5)$$

When gamma rays interact with a material via Compton scattering, secondary photons are produced with energies equal to or lower than the incident photons. These photons deposit their energy into the medium, leading to secondary radiation. This phenomenon can be quantified using the "buildup factor." The Buildup Factor is defined as the ratio of the total radiation value at a specific point within a medium to the contribution of radiation reaching that point without any interaction. There are two types of buildup factors:

Energy Absorption Buildup Factor (EABF) focuses on photon absorption as the quantity of interest. Exposure Buildup Factor (EBF) pertains to the amount of radiation exposure to air after passing through the absorber. These definitions and distinctions are well-documented in the literature (Harima, 1993; Ekinci et al., 2019; Issa et al., 2019). In this study, the EABF and EBF values for the alloys were calculated using the EpiXS program (Hila et al., 2021) employing the Geometric Progression (GP)-Fitting method. Detailed computational steps for these calculations can be found in many previous works (Kavaz, 2019; Abouhaswa & Kavaz, 2020; Kavaz et al., 2020).

3. Results

In this study, the gamma radiation shielding parameters of some selected high entropy alloys FeCoNiCrMn, TaNbHfZrTi, NbMoTaW, AlMoNbV and NbTaTiV (Shang et al., 2021) have been extensively investigated. For this purpose, the mass attenuation coefficients (MAC, cm^2/g) of the selected alloys in a wide photon energy range of 0.015-15 MeV were obtained by EpiXS software (Hila et al., 2021). EpiXS is a specialized software program designed for calculating mass attenuation coefficients and other photon interaction parameters, offering precise computational capabilities for radiation shielding studies. The verification of the obtained results was carried out with the results obtained with WinXCOM software (Gerward et al., 2004). WinXCOM is a widely used software tool for calculating photon cross-sections and mass attenuation coefficients, providing reliable and validated results for various materials. The results are listed in Table 1 and the variation of MAC values with photon energy is presented in Figure 1. From Figure is seen that the change in MAC values shows that the matter interacts with the photon in different ways. Since the photoelectric effect is dominant at low energies, MAC values have the highest values. It is seen that MAC values decrease rapidly as the energy increases. However, small sudden peaks occur around 20 keV and 70 keV. The peaks around 20 keV are the K shell absorption edges of Nb and Mo (18.98 and 19.99 keV) and around 70 keV are the K shell absorption edges of Ta, W and Hf (65, 67 and 69 keV).

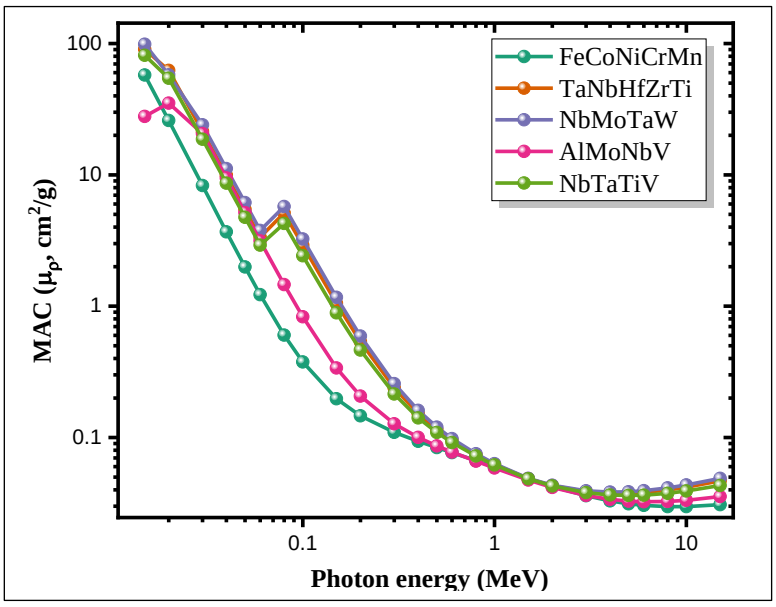

Figure 1. Variation of mass attenuation coefficient (MAC) against photon energy for the HEA samples.

Since the Compton scattering process is active in the medium energy region (Z/E), the MAC values have the lowest values in the 0.4-3 MeV range due to secondary scattering. Beyond 3 MeV, MAC values start to increase again. Since the photon-matter interaction cross-section is proportional to Z^2 in the pair formation process, MAC values increase with the increase in the atomic number of the elements in the alloys. From Table 1, at 0.015 MeV, MAC values are 57.6, 90.4, 98.9, 27.8 and 81.5 cm^2/g for FeCoNiCrMn, TaNbHfZrTi, NbMoTaW, AlMoNbV and NbTaTiV alloys, respectively. NbMoTaW alloy has the highest MAC values, while AlMoNbV has the lowest MAC values.

Figure 2 shows the variation of half value layer (HVL) for selected high entropy alloys. The HVL refers to the half-thickness of a material and is used to assess the radiation shielding capacity of the material. At low energies (up to 0.1 MeV), the HVL values of all alloys are low and very close to each other. As the energy increases (towards 10 MeV), the HVL values of all alloys increase, meaning that at higher energies these materials need to be thicker. The alloy with the highest HVL values is NbMoTaW, while the alloy with the lowest HVL values is AlMoNbV. The NbTaTiV alloy has an average HVL value and shows less HVL increase with increasing energy compared to other alloys. TaNbHfZrTi and FeCoNiCrMn alloys follow a similar trend and have similar HVL values with increasing energy. For high-energy photons, NbMoTaW alloy provides the highest protection, while AlMoNbV alloy is effective at lower energies.

Table 1. Mass attenuation coefficients ($\mu\rho$, cm^2/g) for HEA samples found with EpiXS and WinXCOM

Photon energy (MeV)	**Mass attenuation coefficient(cm^2/g)**									
	FeCoNiCrMn		**TaNbHfZrTi**		**NbMoTaW**		**AlMoNbV**		**NbTaTiV**	
	WinX	**EpiXS**	**WinX**	**EpiXS**	**WinX**	**EpiXS**	**WinX**	**EpiXS**	**WinX**	**EpiXS**
0.015	57.551	57.617	90.771	90.499	99.398	98.911	27.967	27.863	81.795	81.519
0.02	25.938	25.980	62.305	62.406	69.243	57.728	59.210	35.159	54.433	54.516
0.03	8.269	8.289	21.446	21.464	24.037	24.059	20.574	20.600	18.666	18.683
0.04	3.673	3.684	9.960	9.950	11.189	11.176	9.449	9.462	8.653	8.643
0.05	1.982	1.988	5.497	5.469	6.179	6.150	5.143	5.153	4.773	4.752
0.06	1.219	1.223	3.397	3.352	3.816	3.774	3.132	3.142	2.952	2.919
0.08	0.601	0.603	5.126	5.135	5.726	5.736	1.455	1.460	4.258	4.266
0.1	0.375	0.376	2.901	2.908	3.244	3.247	0.828	0.830	2.421	2.424
0.15	0.197	0.197	1.049	1.052	1.166	1.168	0.338	0.338	0.888	0.890
0.2	0.146	0.146	0.536	0.537	0.590	0.592	0.206	0.207	0.462	0.463
0.3	0.110	0.110	0.239	0.239	0.257	0.257	0.127	0.127	0.214	0.214
0.4	0.094	0.094	0.152	0.152	0.161	0.161	0.100	0.100	0.141	0.141
0.5	0.084	0.084	0.115	0.115	0.120	0.120	0.087	0.086	0.109	0.109
0.6	0.077	0.077	0.095	0.095	0.098	0.098	0.078	0.078	0.092	0.092
0.8	0.067	0.067	0.074	0.074	0.075	0.075	0.066	0.066	0.073	0.072
1	0.060	0.060	0.063	0.063	0.063	0.063	0.059	0.059	0.062	0.062
1.5	0.049	0.049	0.049	0.049	0.049	0.049	0.048	0.047	0.049	0.049
2	0.042	0.042	0.043	0.043	0.043	0.043	0.042	0.042	0.043	0.043
3	0.036	0.036	0.039	0.039	0.039	0.039	0.036	0.036	0.038	0.038
4	0.033	0.033	0.038	0.038	0.038	0.038	0.034	0.034	0.037	0.037
5	0.031	0.031	0.038	0.038	0.039	0.039	0.033	0.033	0.036	0.036
6	0.030	0.030	0.038	0.038	0.039	0.039	0.032	0.032	0.036	0.036
8	0.030	0.030	0.040	0.040	0.041	0.041	0.033	0.033	0.038	0.038
10	0.030	0.030	0.042	0.042	0.044	0.044	0.033	0.033	0.039	0.039
15	0.031	0.031	0.047	0.047	0.049	0.049	0.036	0.036	0.043	0.043

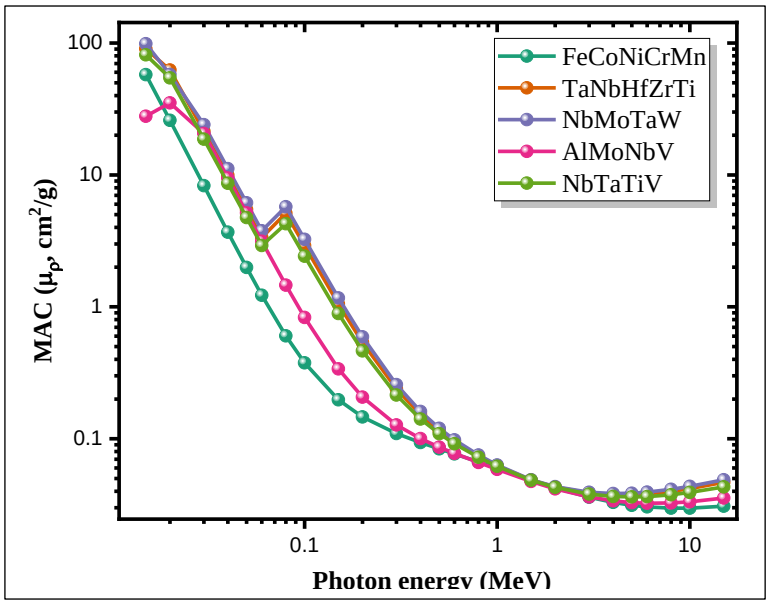

Figure 2. Variation of half value layer (HVL) against photon energy for the HEA samples.

Figure 3 shows the mean free path (MFP) values of the proposed high entropy alloys and conventional shielding materials as a function of photon energy. As with the HVL, at low energies, the MFP values of all materials are low and close to each other. As the energy increases, the MFP values of all materials increase, meaning that at higher energies the photon absorption capacity of these materials decreases. RS520 commercial glass is the conventional material with the best radiation shielding capacity. Conventional shielding materials such as concretes and commercial glasses have moderate MFP values and may be less effective in a given energy range compared to high entropy alloys. NbMoTaW alloy has lower MFP values compared to other high-entropy alloys and conventional materials at all energies, meaning they provide more effective radiation protection. Overall, however, it can be said that all of the selected high-entropy alloys are better than conventional materials in attenuating gamma radiation.

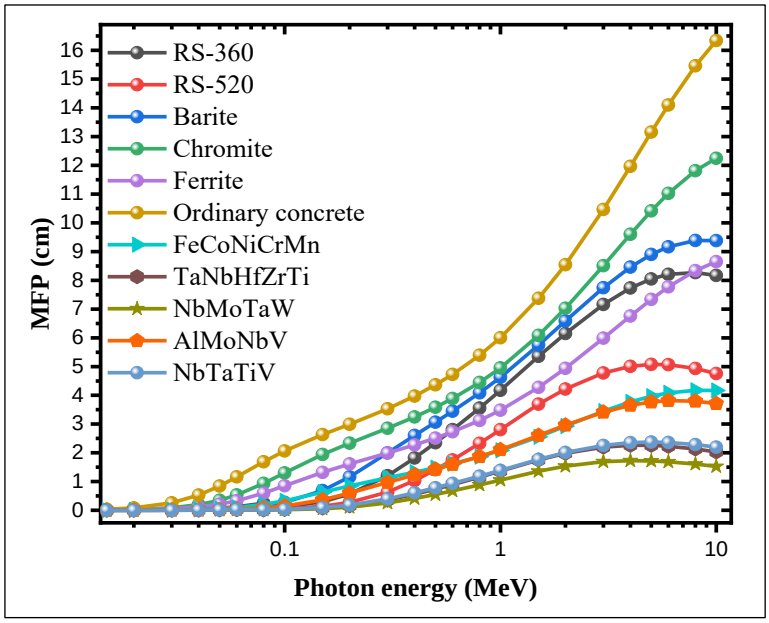

Figure 3. Comparison of MFP values of HEA samples with commonly used shielding materials.

Figure 4 provides a detailed view of how different HEA samples perform in terms of their effective atomic number (Z_{eff}) in the range 0.015-15 MeV of photon energy. In the 0.015-0.1 MeV energy range, Z_{eff} takes the largest values due to the variation of the photoelectric absorption cross-section with Z^{4-5}. Around 20 keV, the Z_{eff} values of Nb and Mo and around 70 keV of Ta, W and Hf show sudden increases due to the K layer absorption edges. At intermediate and high energies, the Z dependence of the photon-matter interaction decreases. Therefore, the Z_{eff} change is slow in these regions. NbMoTaW and TaNbHfZrTi alloys are characterized by high Z_{eff} values in all energy regions. On the other hand, FeCoNiCrMn and NbTaTiV alloys are less effective compared to other alloys with low and constant Z_{eff} values.

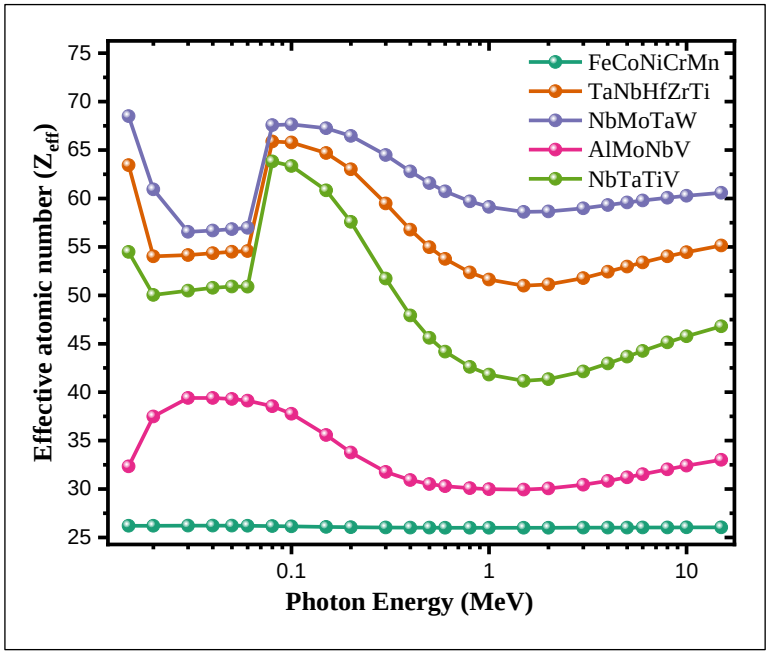

Figure 4. Variation of effective atomic number (Z_{eff}) against photon energy for the HEA samples.

Figure 5 presents the EBF values of five HEAs over a wide range of photon energies at penetration depths of 1-15 mfp. For all samples, the EBF starts from a lower value at the lowest energies, increases to a peak as the energy increases and decreases again at higher energies. Except for FeCoNiCrMn, for the other alloys there is a sharp increase in EBF values at low photon energies (around 0.02 and 0.07 MeV), indicating high interaction and accumulation. These increases are due to the absorption edges of the high atomic number elements in the four alloys. The peak of the EBF shifts to lower energies as the thickness of the material increases. This indicates that for thicker materials, the maximum exposure buildup occurs at lower photon energies. As the material becomes thicker (more MFP), the peak EBF value becomes higher. This means that thicker materials have a greater buildup factor, likely due to more opportunities for photons to scatter within the material. The initial rise, peak, and subsequent fall of the EBF with energy result from the complex interaction between different types of photon interactions with matter, such as photoelectric absorption, Compton scattering, and pair production. At low energies, FeCoNiCrMn alloy has the lowest EBF values. NbMoTaW and TaNbHfZrTi alloys, which have the highest Z_{eff} values in the medium energy range, have the lowest EBF values and are the best radiation absorbers. At high energies, since the photon-matter interaction changes with Z^2, FeCoNiCrMn and AlMoNbV alloys with the lowest Z_{eff} values have the lowest EBF values. When all radiation shielding parameters are examined, NbMoTaW and TaNbHfZrTi alloys have higher usability as radiation shields.

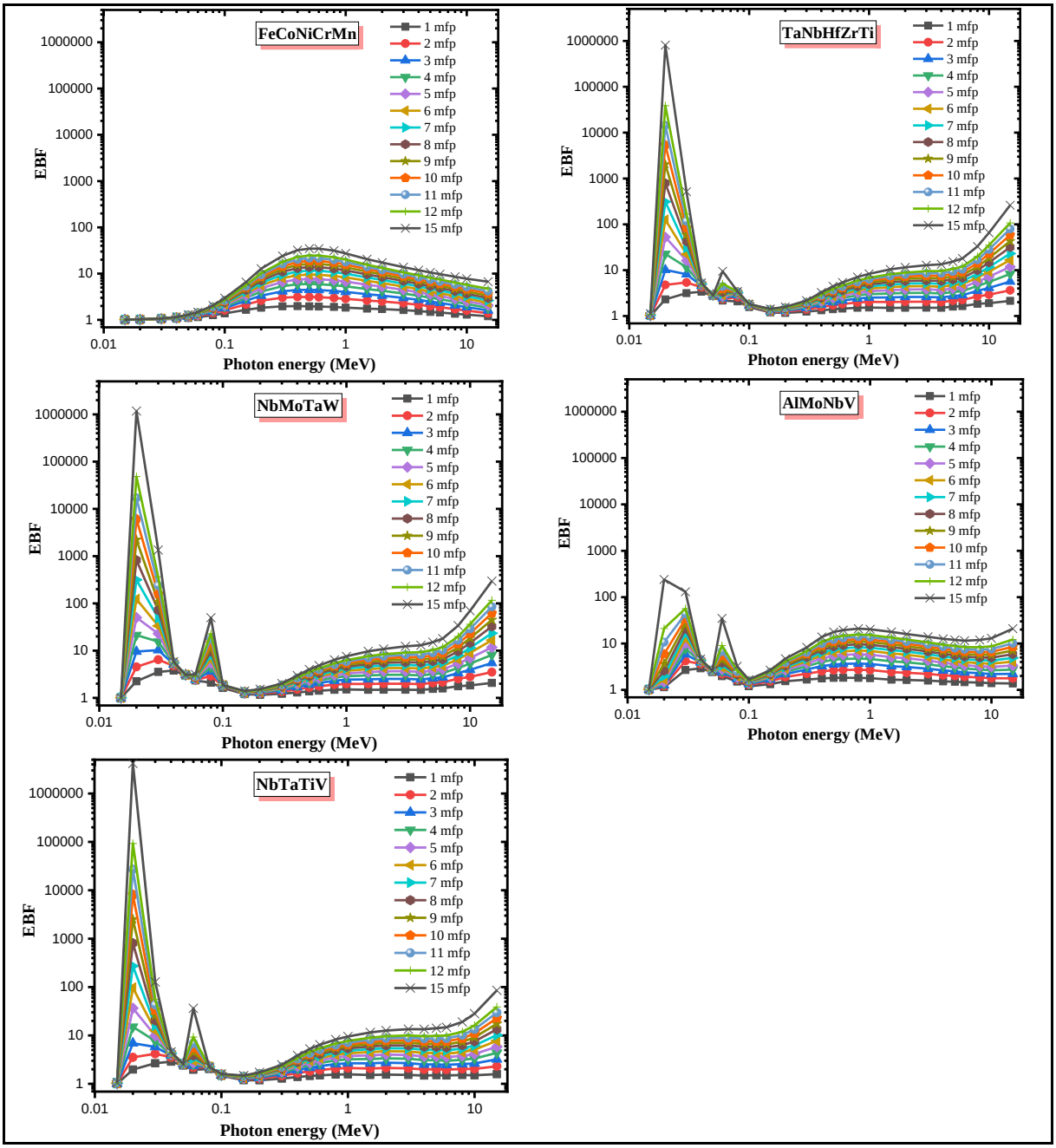

Figure 5. Variation of exposure build-up factors (EBF) against photon energy at different penetration depths for HEA samples.

4. Discussion and Conclusion

This study provides a comprehensive evaluation of the gamma radiation shielding capabilities of selected high entropy alloys (HEAs), namely FeCoNiCrMn, TaNbHfZrTi, NbMoTaW, AlMoNbV, and NbTaTiV. The key findings are as follows:

1. The MAC values were calculated using the EpiXS program across a photon energy range of 0.015-15 MeV and were verified using WinXCOM software. The results indicate that MAC values are highest at low photon energies due to the photoelectric effect, with notable peaks corresponding to the K-shell absorption edges of specific elements. Alloys containing heavy elements were found to have larger MAC values. For 0.015 MeV, the MAC for the FeCoNiCrMn, TaNbHfZrTi, NbMoTaW, AlMoNbV, and NbTaTiV alloys are 57.6, 90.4, 98.9, 27.8, and 81.5 cm^2/g, respectively. Among these alloys, NbMoTaW demonstrates the highest MAC value, while AlMoNbV shows the lowest.

2. The HVL and MFP values suggest that thicker HEA samples are required to achieve effective shielding at higher photon energies. Specifically, NbMoTaW showed the highest MAC and lowest HVL values, indicating superior shielding capabilities, while AlMoNbV have the lowest.
3. The effective atomic number (Z_{eff}) and EBF analyses revealed that NbMoTaW and TaNbHfZrTi alloys have higher radiation shielding potential compared to conventional materials. These alloys exhibited higher Z_{eff} values across all energy regions, suggesting better photon interaction and absorption characteristics.
4. Among the studied alloys, NbMoTaW and TaNbHfZrTi demonstrated the best overall performance in gamma radiation shielding. They provide higher usability in environments subjected to gamma radiation, outperforming traditional shielding materials.

The findings from this study underscore the potential of HEAs in advanced shielding applications. Their unique combination of high MAC values at low energies, lower HVL and MFP values at higher energies, and superior Z_{eff} and EBF performance makes them promising candidates for enhancing safety and performance in sectors requiring effective radiation shielding. Furthermore, this study demonstrates the superior radiation shielding capabilities of HEAs by establishing the comparative performance of selected HEAs with conventional shielding materials. This provides an important benchmark for future studies and highlights the superior performance of HEAs.

References

Abouhaswa, A. S., & Kavaz, E. (2020). Bi_2O_3 effect on physical, optical, structural and radiation safety characteristics of B_2O_3-Na_2O-ZnO-CaO glass system. *Journal of Non-Crystalline Solids*, 535, 119993. https://doi.org/10.1016/j.jnoncrysol.2020.119993

Buluc, G., Chelariu, R., Popescu, G., Sârghi, M., & Carcea, I. (2017). Study on wear resistance FeNiCrMnAl high entropy alloy - Mechanical properties. *Key Engineering Materials*, *750*, 34-38. https://doi.org/10.4028/www.scientific.net/KEM.750.34

Ekinci, N., Kavaz, E., Aygün, B., & Perişanoğlu, U. (2019). Gamma ray shielding capabilities of rhenium-based superalloys. *Radiation Effects and Defects in Solids*, *174*(5-6), 435-451. https://doi.org/10.1080/10420150.2019.1596110

Ferreirós, P. A., von Tiedemann, S. O., Parkes, N., Gurah, D., King, D. J. M., Norman, P., … & Knowles, A. J. (2023). VNbCrMo refractory high-entropy alloy for nuclear applications. *International Journal of Refractory Metals and Hard Materials*, *113*, 106200. https://doi.org/10.1016/j.ijrmhm.2023.106200

Filho, F. da C. G., da Luz, F. S., da Silva Figueiredo, A. B.-H., Monteiro, S. N., & dos Santos, D. S. (2020). Promising ballistic behavior of CoCrFeMnNi high entropy alloy. *Materials Science Forum*, *1012*, 377-382. https://doi.org/10.4028/www.scientific.net/MSF.1012.377

Gerward, L., Guilbert, N., Jensen, K. B., & Levring, H. (2004). WinXCom—a program for calculating X-ray attenuation coefficients. *Radiation Physics and Chemistry*, *71*(3-4), 653-654. https://doi.org/10.1016/j.radphyschem.2004.04.040

Harima, Y. (1993). An historical review and current status of buildup factor calculations and applications. *Radiation Physics and Chemistry*, *41*(4-5), 631-672. https://doi.org/10.1016/0969-806X(93)90317-N

Hila, F. C., Asuncion-Astronomo, A., Dingle, C. A. M., Jecong, J. F. M., Javier-Hila, A. M. V., Gili, M. B. Z., … & Amorsolo, A. V. (2021). EpiXS: A windows-based program for photon attenuation, dosimetry and shielding based on EPICS2017 (ENDF/B-VIII) and EPDL97 (ENDF/B-VI.8). *Radiation Physics and Chemistry*, *182*, 109331. https://doi.org/10.1016/j.radphyschem.2020.109331

Issa, S. A. M., Ahmad, M., Tekin, H. O., Saddeek, Y. B., & Sayyed, M. I. (2019). Effect of Bi_2O_3 content on mechanical and nuclear radiation shielding properties of Bi_2O_3-MoO_3-B_2O_3-SiO_2-Na_2O-Fe_2O_3 glass system. *Results in Physics*, *13*, 102165. https://doi.org/10.1016/j.rinp.2019.102165

Issa, S. A. M., Rashad, M., Zakaly, H. M. H., Tekin, H. O., & Abouhaswa, A. S. (2020). Nb2O5-Li2O-Bi2O3-B2O3 novel glassy system: evaluation of optical, mechanical, and gamma shielding parameters. *Journal of Materials Science: Materials in Electronics*, *31*(24), 22039-22056. https://doi.org/10.1007/s10854-020-04707-7

Jia, N., Li, Y., Huang, H., Chen, S., Li, D., Dou, Y., … & Jin, K. (2021). Helium bubble formation in refractory single-phase concentrated solid solution alloys under MeV He ion irradiation. *Journal of Nuclear Materials*, *550*, 152937. https://doi.org/10.1016/j.jnucmat.2021.152937

Kavaz, E. (2019). An experimental study on gamma ray shielding features of lithium borate glasses doped with dolomite, hematite and goethite minerals. *Radiation Physics and Chemistry*, *160*, 112-123. https://doi.org/10.1016/j.radphyschem.2019.03.032

Kavaz, E., Armoosh, S. R., Perişanoğlu, U., Ahmadi, N., & Oltulu, M. (2020). Gamma ray shielding effectiveness of the Portland cement pastes doped with brass-copper: An experimental study. *Radiation Physics and Chemistry*, *166*, 108526. https://doi.org/10.1016/j.radphyschem.2019.108526

Kavaz, E., Gul, A. O., Basgoz, O., Guler, O., ALMisned, G., Bahceci, E., … & Tekin, H. O. (2022). Boron nitride nanosheet-reinforced WNiCoFeCr high-entropy alloys: the role of B4C on the structural, physical, mechanical, and radiological shielding properties. *Applied Physics A*, *128*(8), 694. https://doi.org/10.1007/s00339-022-05813-5

Lu, Y., Huang, H., Gao, X., Ren, C., Gao, J., Zhang, H., … & Li, T. (2019). A promising new class of irradiation tolerant materials: Ti2ZrHfV0.5Mo0.2 high-entropy alloy. *Journal of Materials Science & Technology*, *35*(3), 369-373. https://doi.org/10.1016/j.jmst.2018.09.034

Lu, Z. P., Wang, H., Chen, M. W., Baker, I., Yeh, J. W., Liu, C. T., & Nieh, T. G. (2015). An assessment on the future development of high-entropy alloys: Summary from a recent workshop. *Intermetallics*, *66*, 67-76. https://doi.org/10.1016/j.intermet.2015.06.021

Müller, F., Gorr, B., Christ, H.-J., Müller, J., Butz, B., Chen, H., … & Heilmaier, M. (2019). On the oxidation mechanism of refractory high entropy alloys. *Corrosion Science*, *159*, 108161. https://doi.org/10.1016/j.corsci.2019.108161

Perişanoğlu, U., Kavaz, E., Tekin, H. O., Armoosh, S. R., Ekinci, N., & Oltulu, M. (2020). Comparison of gamma and neutron shielding competences of Fe–Cu- and brass-added Portland cement pastes: an experimental and Monte Carlo study. *Applied Physics A: Materials Science and Processing*, *126*, 470. https://doi.org/10.1007/s00339-020-03648-6

Rammah, Y. S., Mahmoud, K. A., Kavaz, E., Kumar, A., & El-Agawany, F. I. (2020). The role of PbO/Bi2O3 insertion on the shielding characteristics of novel borate glasses. *Ceramics International*, *46*(15), 23357-23368. https://doi.org/10.1016/j.ceramint.2020.04.018

Ren, H., Chen, R. R., Gao, X. F., Liu, T., Qin, G., Wu, S. P., & Guo, J. J. (2022). Insights on mechanical properties of dual-phase high entropy alloys via Y introduction. *Journal of Alloys and Compounds*, *929*, 167374. https://doi.org/10.1016/j.jallcom.2022.167374

Shang, Y., Brechtl, J., Pistidda, C., & Liaw, P. K. (2021). Mechanical behavior of high-entropy alloys: A review. In J. Brechtl, & P. K. Liaw (Eds.), *High-Entropy Materials: Theory, Experiments, and Applications* (pp. 435-522). Springer.

Socorro-Perdomo, P., Florido-Suarez, N., Voiculescu, I., & Mirza-Rosca, J. (2021). Biocompatibility of new high-entropy alloys with non-cytotoxic elements. *Microscopy and Microanalysis*, *27*(S1), 1772-1774. https://doi.org/10.1017/S1431927621006486

Tunes, M. A., Vo, H. T., Baldwin, J. K. S., Saleh, T. A., Fensin, S. J., & El-Atwani, O. (2023). Perspectives on novel refractory amorphous high-entropy alloys in extreme environments. *Applied Materials Today*, *32*, 101796. https://doi.org/10.1016/j.apmt.2023.101796

Yaykaşlı, H., Eskalen, H., Kavun, Y., Göğebakan, M., & Kaya, A. H. (2023a). Microstructure and thermal and radiation shielding properties of CoCrFeNiAg high entropy alloy. *Journal of Materials Engineering and Performance*, . https://doi.org/10.1007/s11665-023-08598-7

Yaykaşlı, H., Eskalen, H., Kavun, Y., Göğebakan, M., Kaya, A. H., & Yorulmaz, N. (2023b). CoCrFeNiSi high entropy alloy: Synthesis, structural and radiation shielding properties. *Progress in Nuclear Energy*, *165*, 104930. https://doi.org/10.1016/j.pnucene.2023.104930

Yıldız Yorgun, N. (2019). Gamma-ray shielding parameters of $Li_2B_4O_7$ glasses: Undoped and doped with magnetite, siderite and Zinc-Borate minerals cases. *Radiochimica Acta*, *107*(8), 755-765. https://doi.org/10.1515/ract-2019-0014

Zhang, Z., Han, E.-H., & Xiang, C. (2021). Irradiation behaviors of two novel single-phase bcc-structure high-entropy alloys for accident-tolerant fuel cladding. *Journal of Materials Science & Technology*, *84*, 230-238. https://doi.org/10.1016/j.jmst.2020.12.058